

# Supplemental material for Bayesian truncation errors in chiral effective field theory: nucleon-nucleon observables

J. A. Melendez,<sup>\*</sup> S. Wesolowski,<sup>†</sup> and R. J. Furnstahl<sup>‡</sup>  
*Department of Physics, The Ohio State University, Columbus, OH 43210, USA*  
(Dated: August 24, 2017)

Additional figures documenting the conclusions in this paper.

---

<sup>\*</sup> melendez.27@osu.edu  
<sup>†</sup> wesolowski.14@osu.edu  
<sup>‡</sup> furnstahl.1@osu.edu

## I. SUPPLEMENTAL MATERIAL

Here we collect additional informative figures to supplement those in the text.

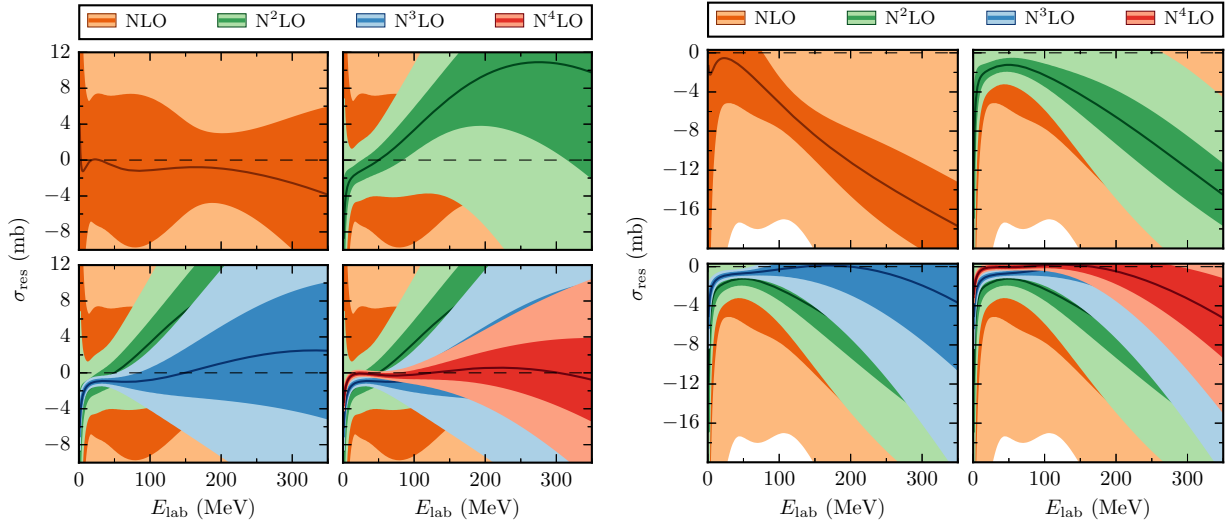


FIG. 1. Residuals at each order for the total  $np$  cross section with DoB intervals calculated using prior set  $C_{0.25-10}$  and  $\Lambda_b = 600$  MeV. Left:  $R = 0.8$  fm, and right:  $R = 1.0$  fm.

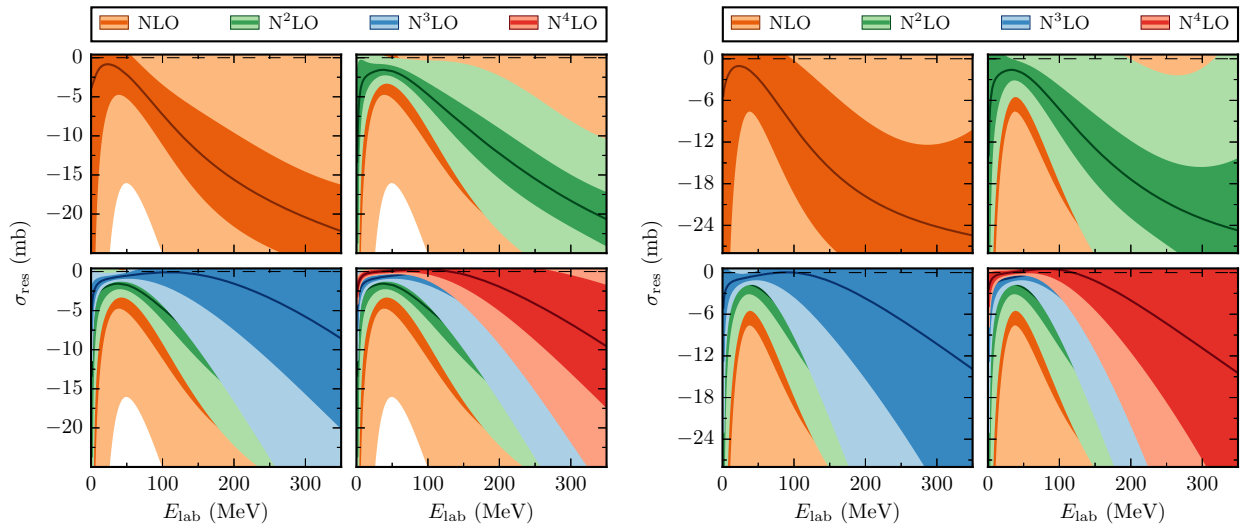


FIG. 2. Residuals at each order for the total  $np$  cross section with DoB intervals calculated using prior set  $C_{0.25-10}$ . Left:  $R = 1.1$  fm with  $\Lambda_b = 500$  MeV, and right:  $R = 1.2$  fm with  $\Lambda_b = 400$  MeV.

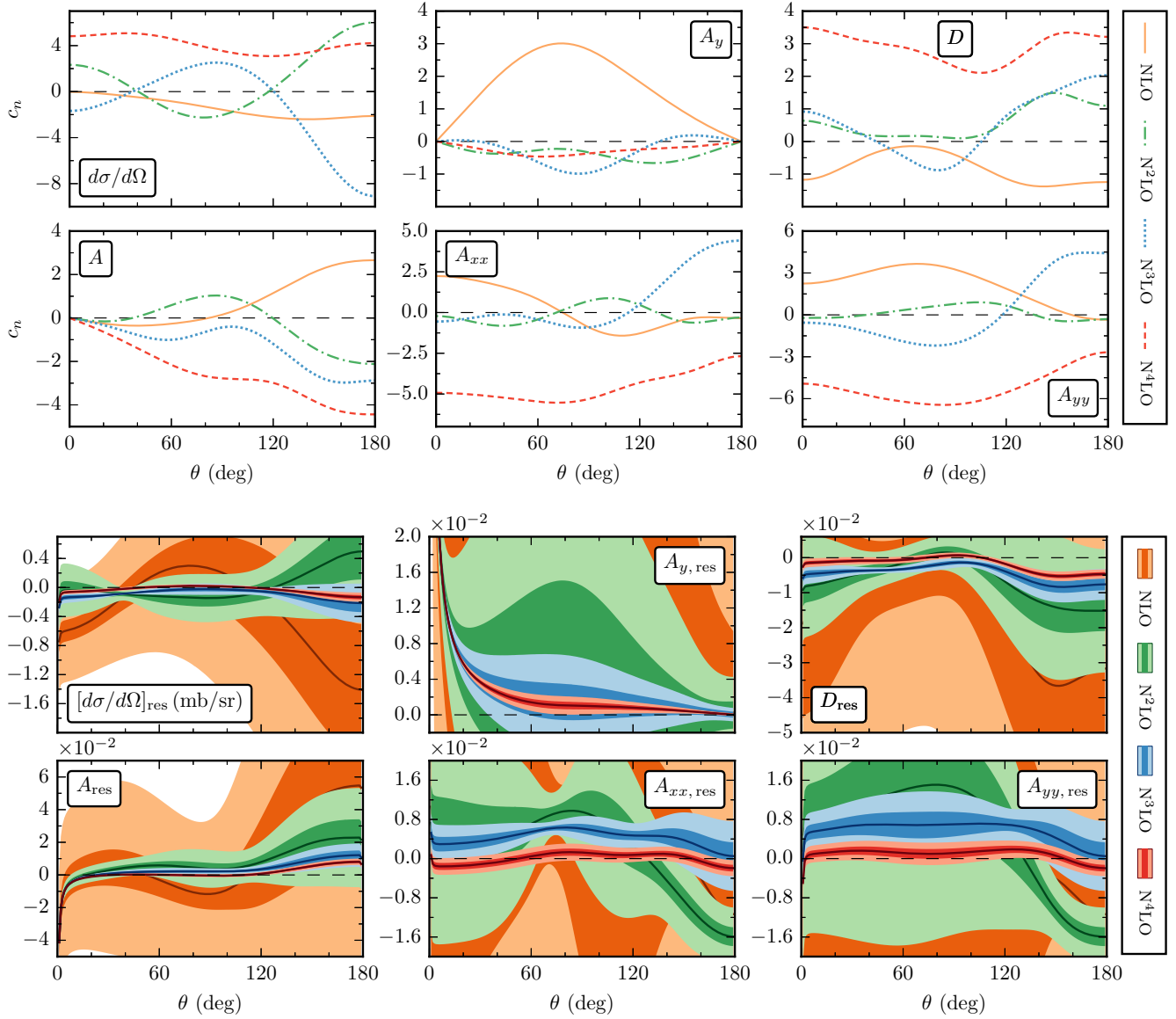


FIG. 3. Top: Observable coefficients for  $E_{\text{lab}} = 50$  MeV with  $X_{\text{ref}} = X_0$  for the differential cross section and  $X_{\text{ref}} = 1$  for all other spin observables. Bottom: Residuals with error bands generated using prior set  $C_{0.25-10}$ .

TABLE I. Observable coefficients  $b_n$  for the  $np$  total cross section in units of  $\text{MeV}^{-n}$ . Lab energy  $E_{\text{lab}}$  and relative momentum  $p_{\text{rel}}$  are in units of MeV.

$E_{\text{lab}}$	$p_{\text{rel}}$	$b_2 \times 10^6$	$b_3 \times 10^9$	$b_4 \times 10^{12}$	$b_5 \times 10^{15}$
50	153	-4.24	0.763	-1.82	50.2
96	212	-2.63	4.14	-4.86	14.7
143	259	-0.975	5.77	-2.18	2.53
200	307	0.300	6.66	2.07	-5.70
300	375	1.26	6.24	8.64	-11.4

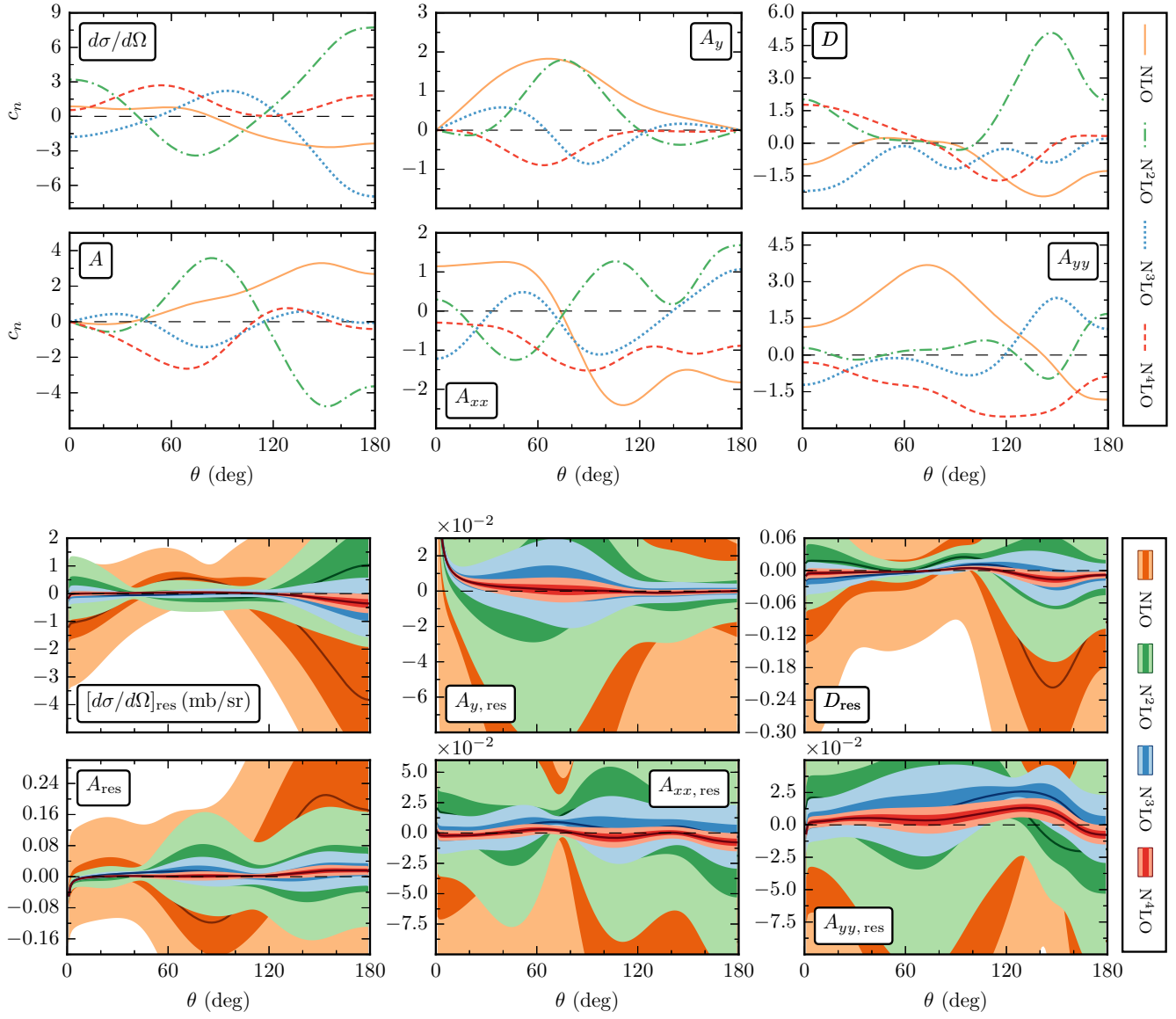


FIG. 4. Same as Fig. 3, but with  $E_{\text{lab}} = 96$  MeV.

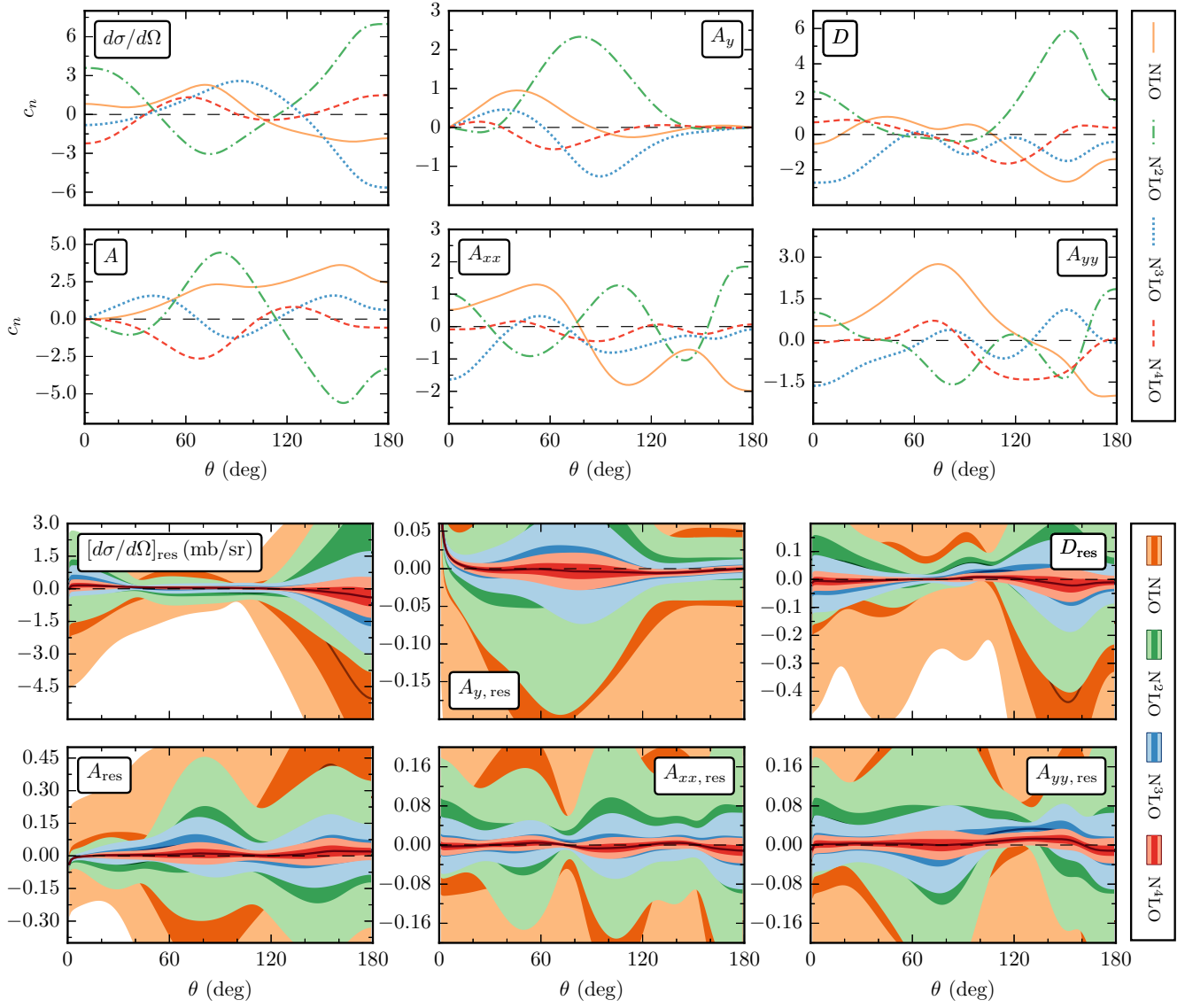


FIG. 5. Same as Fig. 3, but with  $E_{\text{lab}} = 143$  MeV.

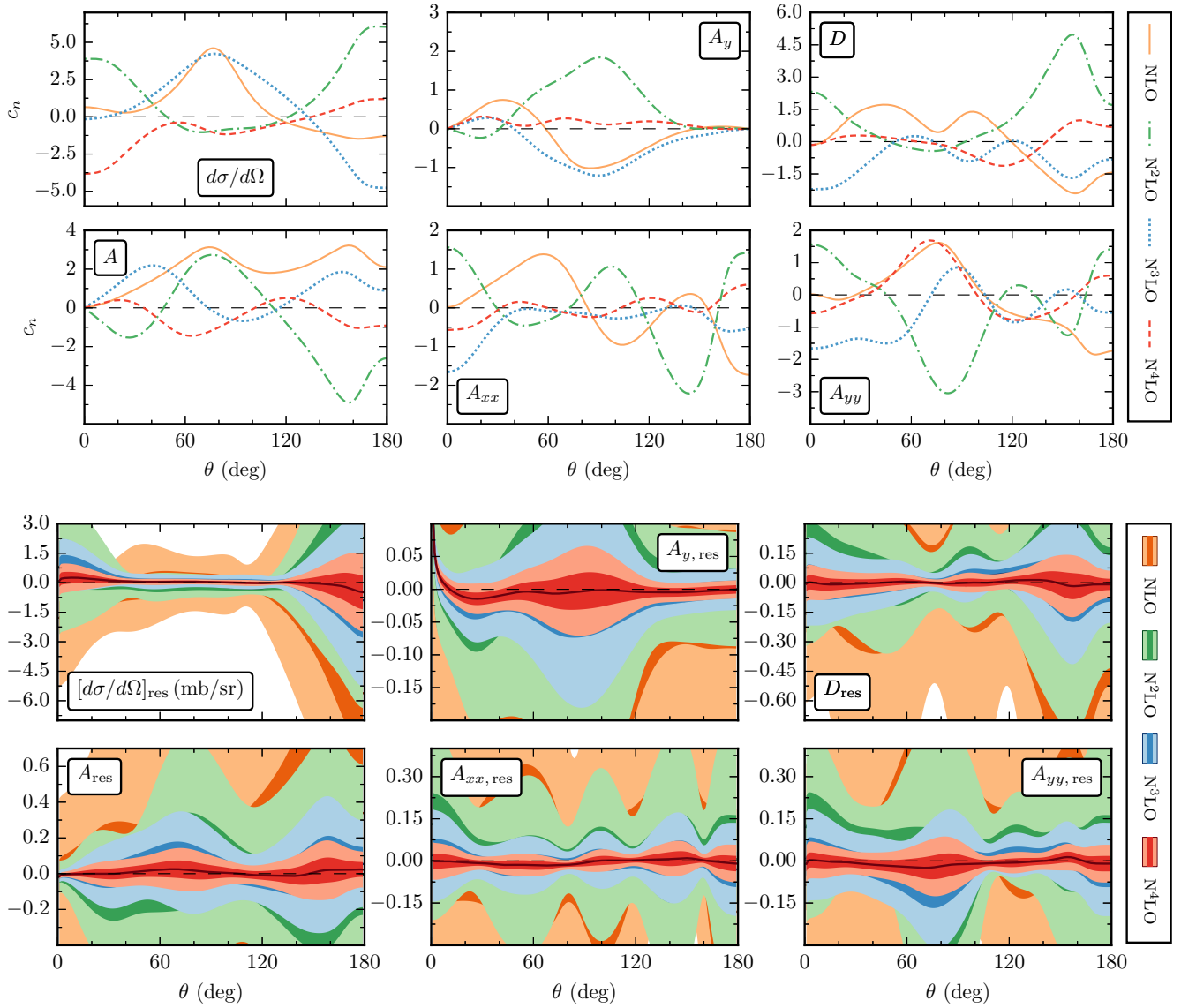


FIG. 6. Same as Fig. 3, but with  $E_{\text{lab}} = 200$  MeV.

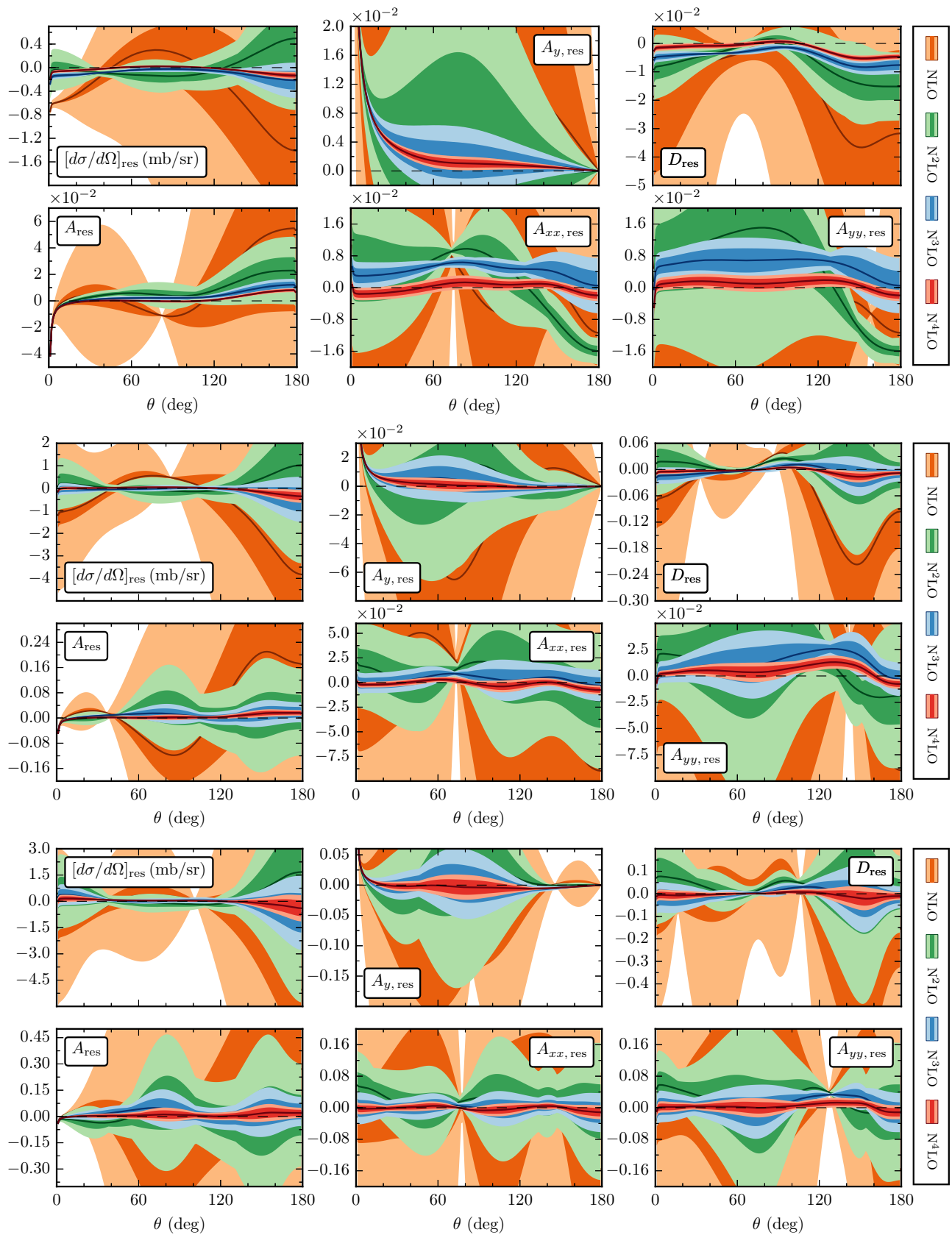


FIG. 7. Residuals computed using the  $R = 0.9$  fm EKM potential with DoBs generated using  $A_\epsilon^{(1)}$ . Top, middle, and bottom plot use  $E_{\text{lab}} = 50, 96, 143$  MeV, respectively.

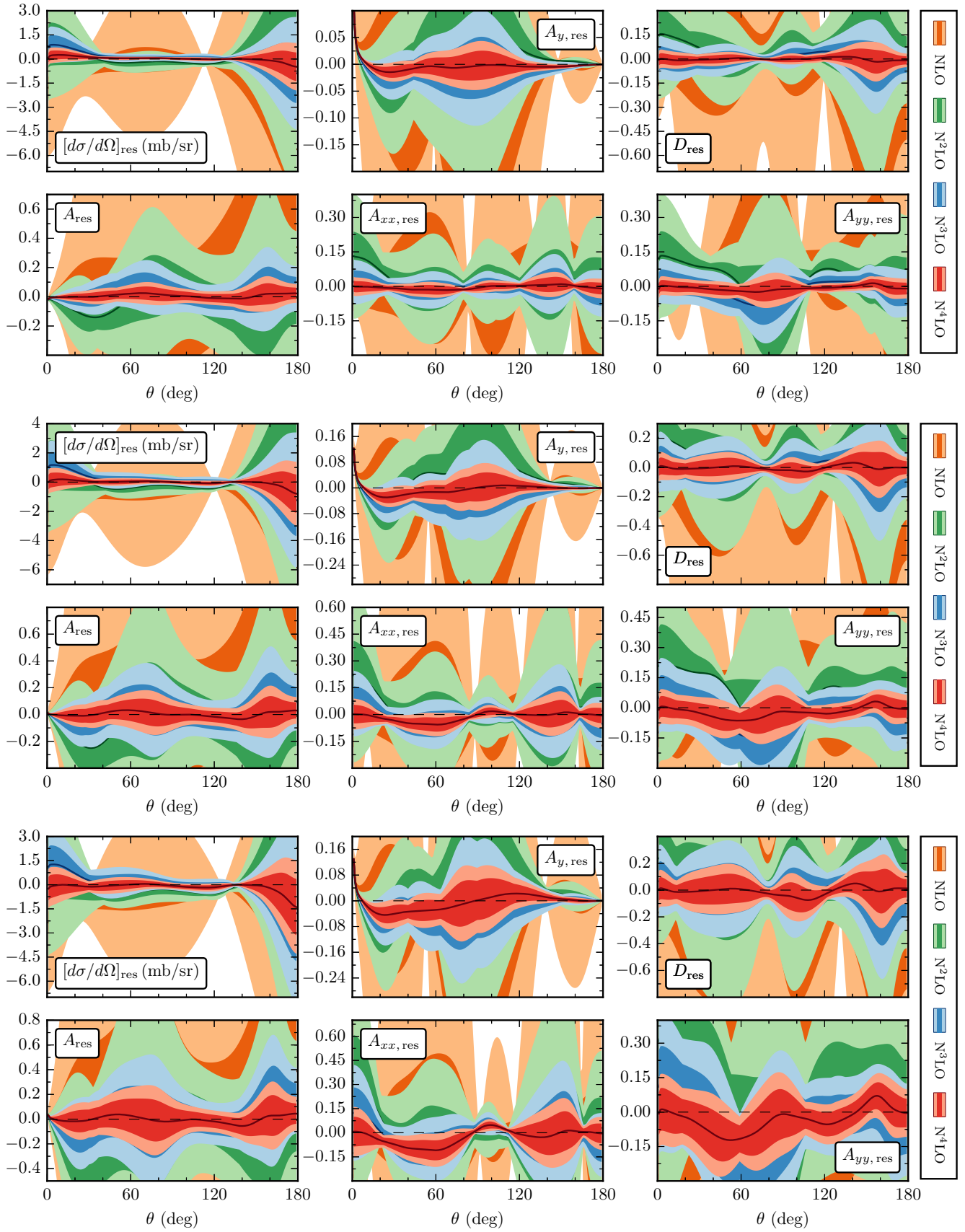


FIG. 8. Same as Fig. 7, but the top, middle, and bottom plot use  $E_{\text{lab}} = 200, 250, 300$  MeV, respectively.



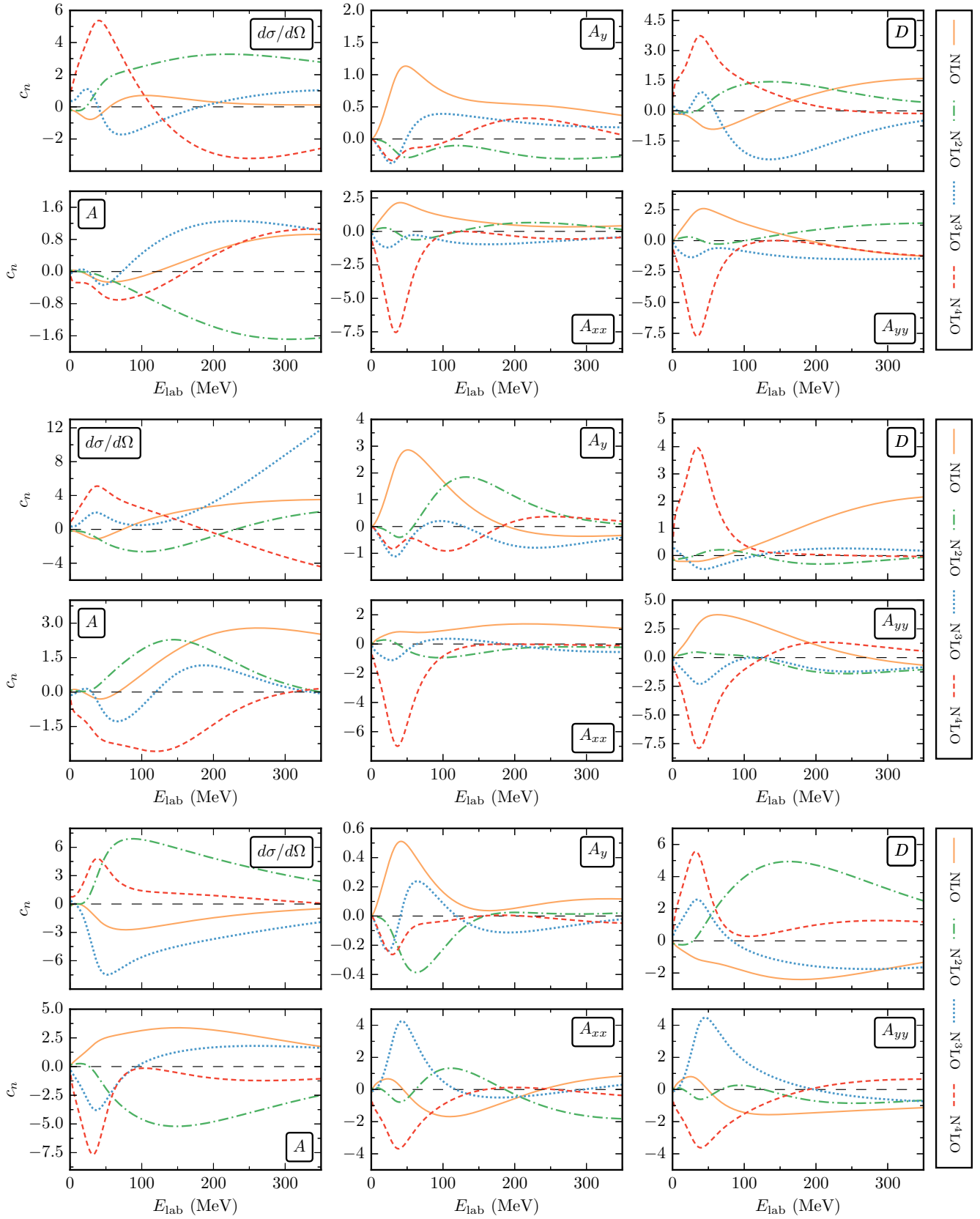


FIG. 9. Coefficients for various angle-dependent observables vs  $E_{\text{lab}}$  using the  $R = 0.9$  fm EKM potential. Top, center, and bottom plots use  $\theta = 20^\circ, 60^\circ, 160^\circ$ , respectively.

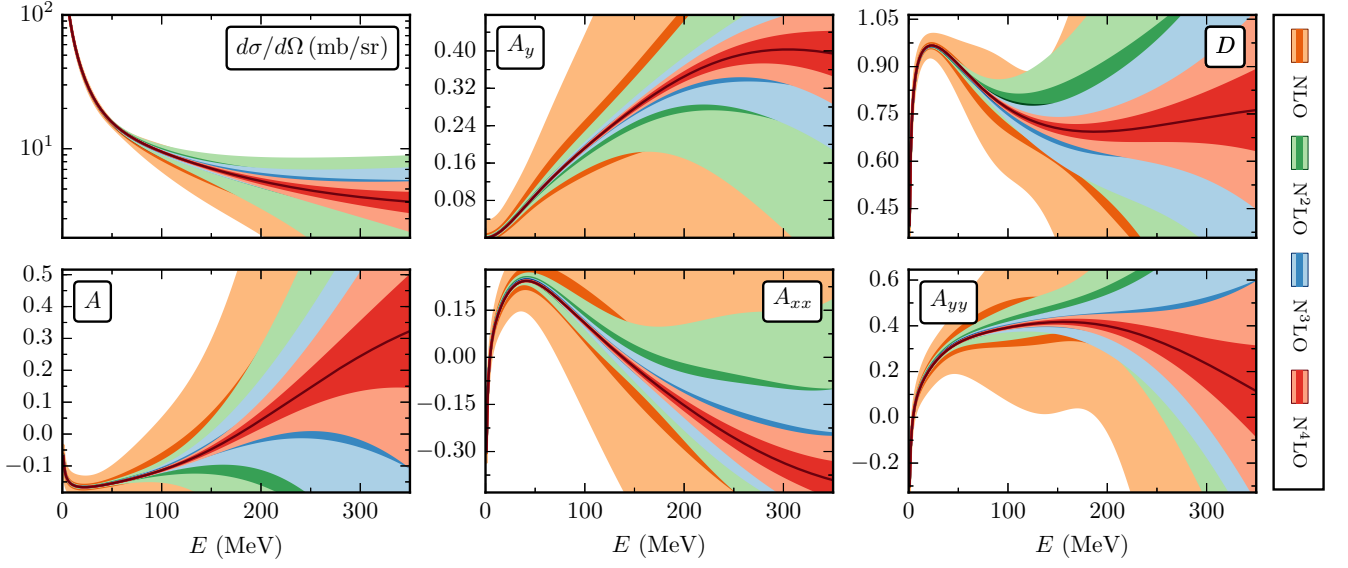


FIG. 10. Observables at  $\theta = 20^\circ$  generated using the  $R = 0.9$  fm EKM potential with error bands from prior set  $C_{0.25-10}$ .

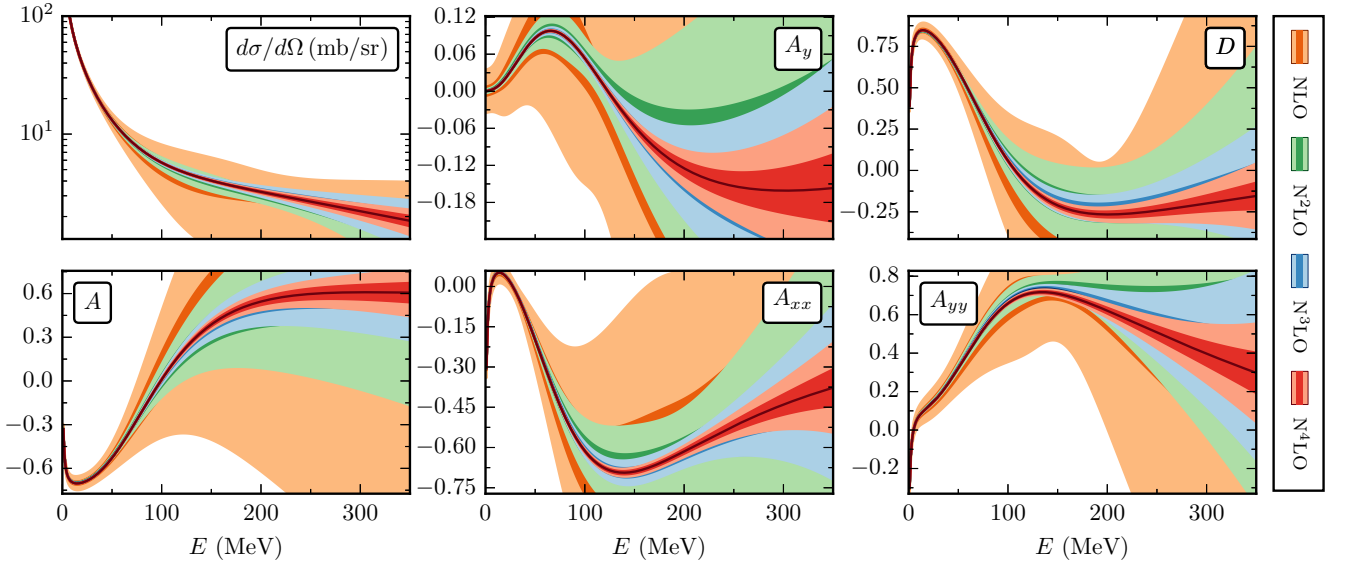


FIG. 11. Observables at  $\theta = 120^\circ$  generated using the  $R = 0.9$  fm EKM potential with error bands from prior set  $C_{0.25-10}$ .

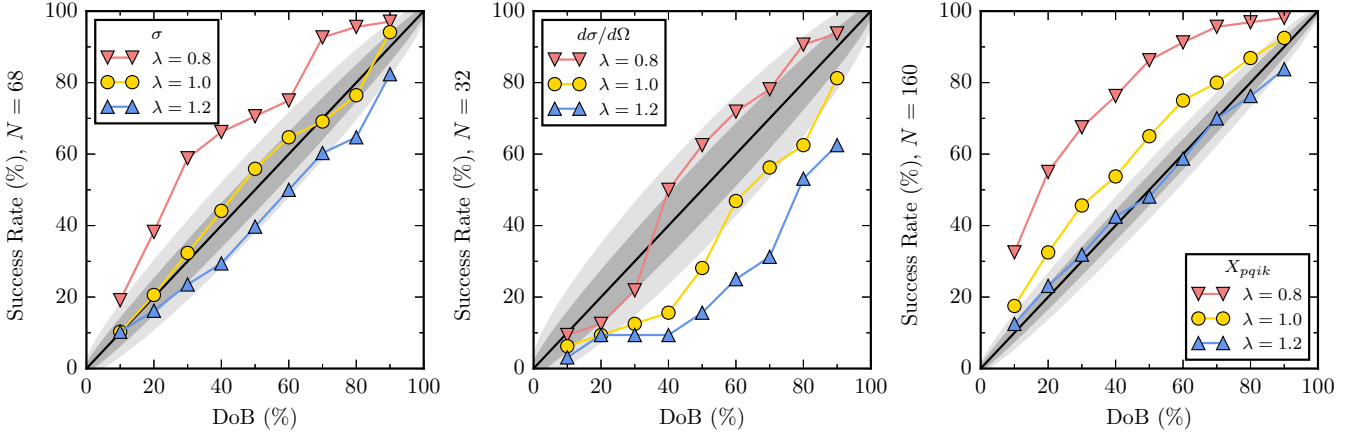


FIG. 12. Consistency plots comparing the NLO–N<sup>4</sup>LO averaged error band success rate to NPWA data for  $R = 0.9$  fm and prior set  $C_{0.25-10}$ . The total cross section is evaluated at  $E_{\text{lab}} = 20, 40, \dots, 340$  MeV, while the rest are evaluated at  $E_{\text{lab}} = 96, 143, 200, 300$  MeV and  $\theta = 60^\circ, 120^\circ$ .

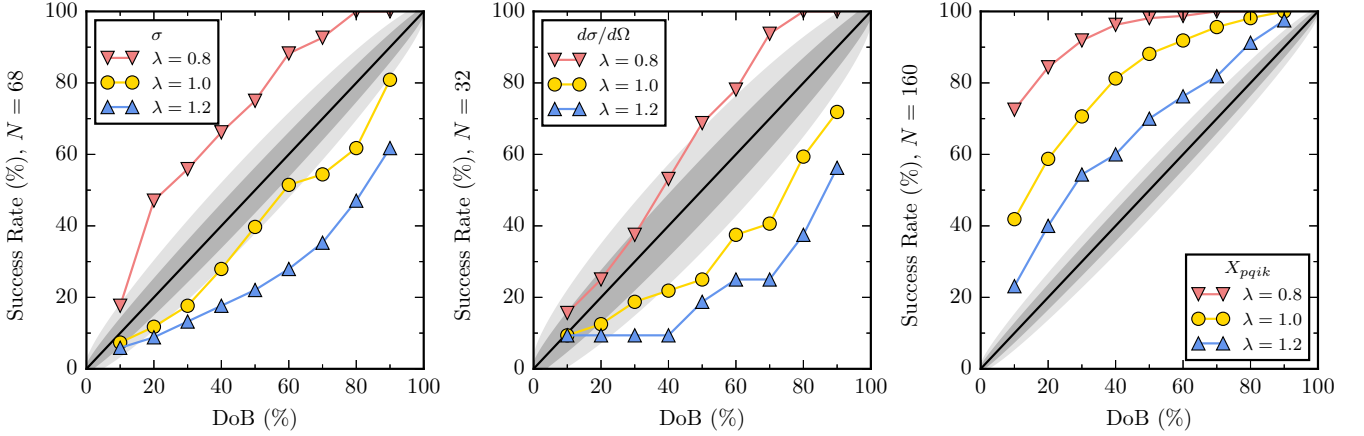


FIG. 13. Consistency plots as in Fig. 12, but with  $R = 1.2$  fm.

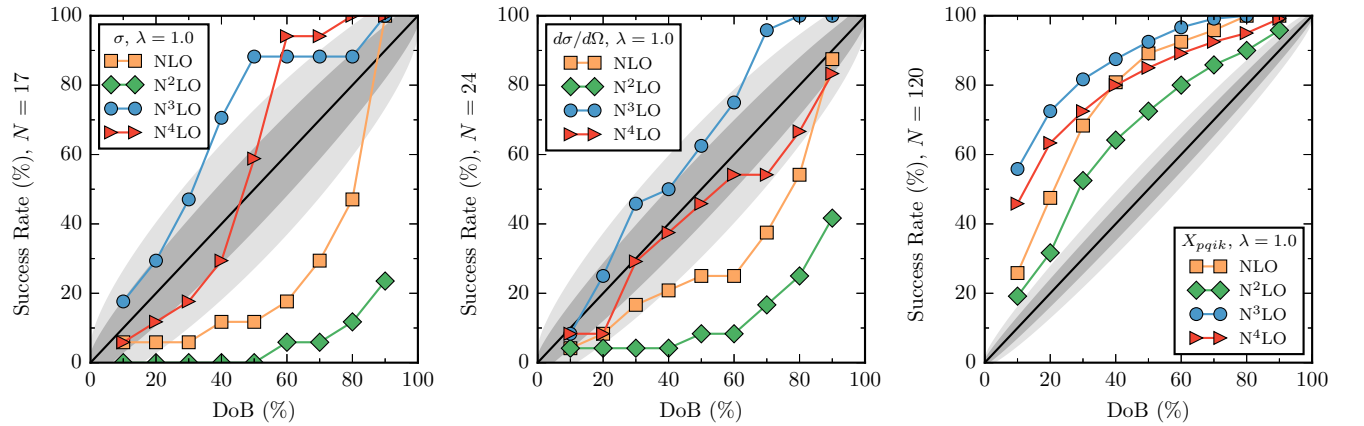
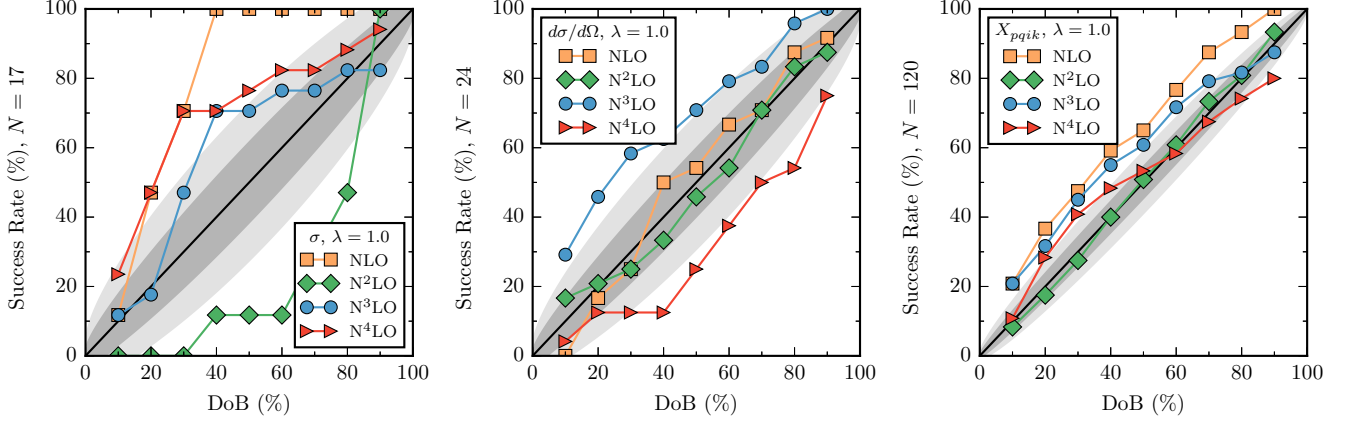
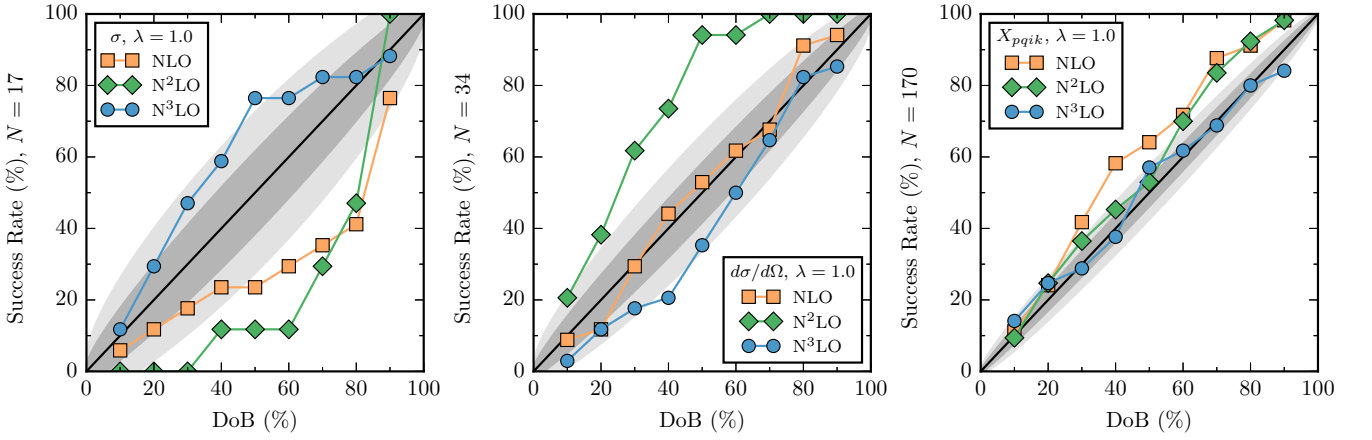
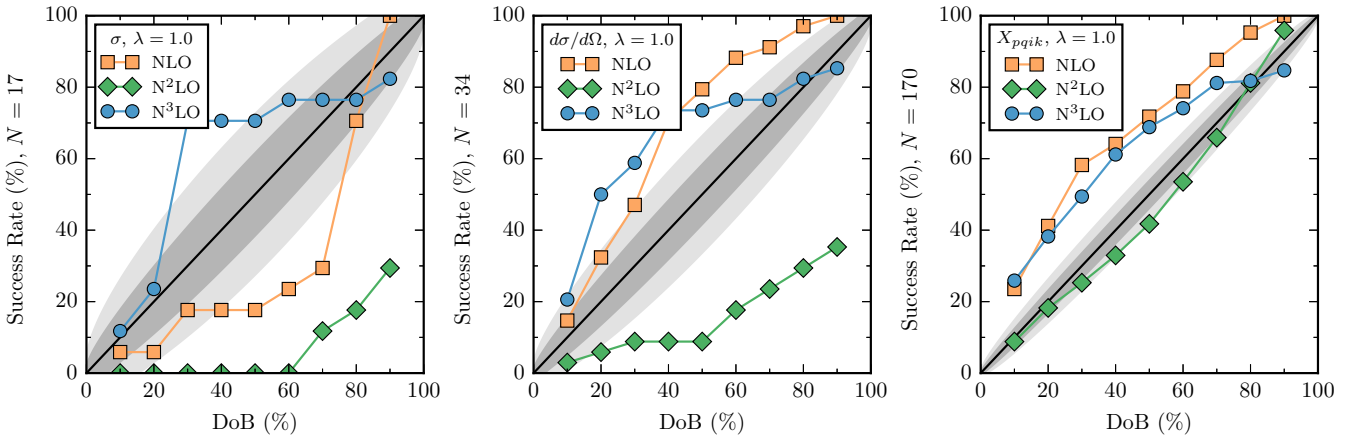


FIG. 14. Consistency plots comparing the order-by-order NLO–N<sup>4</sup>LO error band success rate to NPWA data for  $R = 1.2$  fm and prior set  $C_{0.25-10}$ . The total cross section is evaluated at  $E_{\text{lab}} = 20, 40, \dots, 340$  MeV, while the rest are evaluated at  $E_{\text{lab}} = 96, 143, 200, 300$  MeV and  $\theta = 40^\circ, 60^\circ, \dots, 140^\circ$ .

FIG. 15. Same as Fig. 14 but with  $R = 0.8$  fm.FIG. 16. Consistency plots with the  $R = 0.8$  fm EKM potential showing order-by-order results for  $C_{0.25-10}^{(1)}$ . Here  $\theta = 60^\circ, 120^\circ$  and  $E_{\text{lab}} = 20, 40, \dots, 340$  MeV.FIG. 17. Consistency plots with the  $R = 1.0$  fm EKM potential showing order-by-order results for  $C_{0.25-10}^{(1)}$ . Here  $\theta = 60^\circ, 120^\circ$  and  $E_{\text{lab}} = 20, 40, \dots, 340$  MeV.

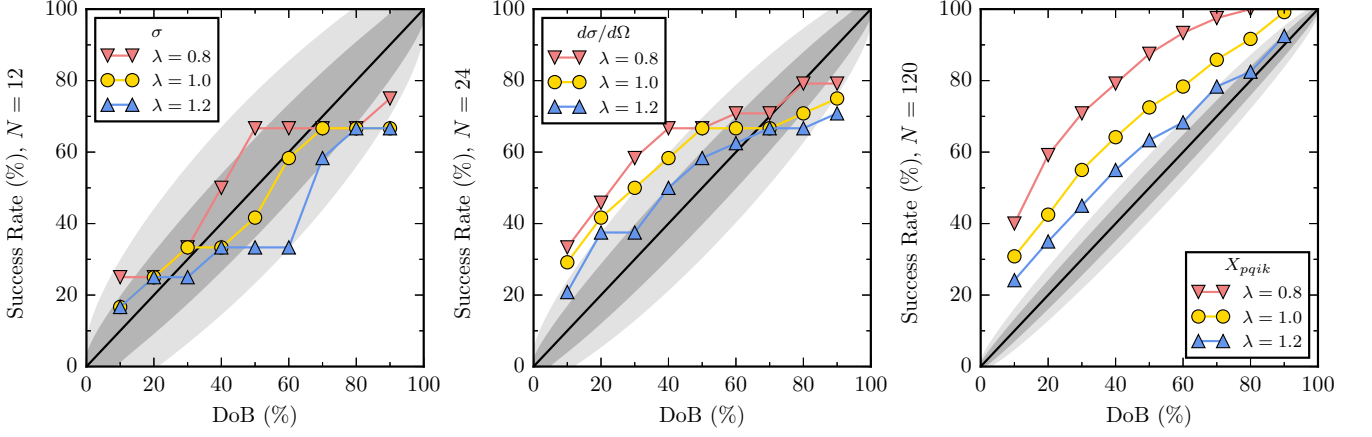


FIG. 18. Consistency plots using  $C_{0.25-10}^{(1)}$  averaged over NLO–N<sup>3</sup>LO results for various observable sets with  $R = 1.1$  fm. Observables are evaluated at  $E_{\text{lab}} = 96, 143, 200, 300$  MeV and at  $\theta = 60^\circ, 120^\circ$  if applicable.

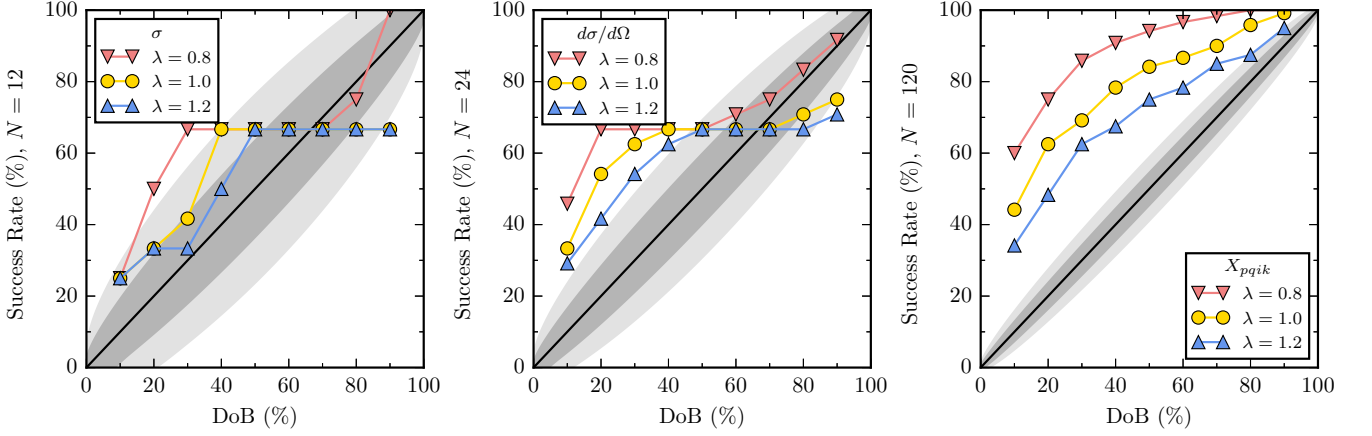


FIG. 19. Same as Fig. 18, but with  $R = 1.2$  fm.

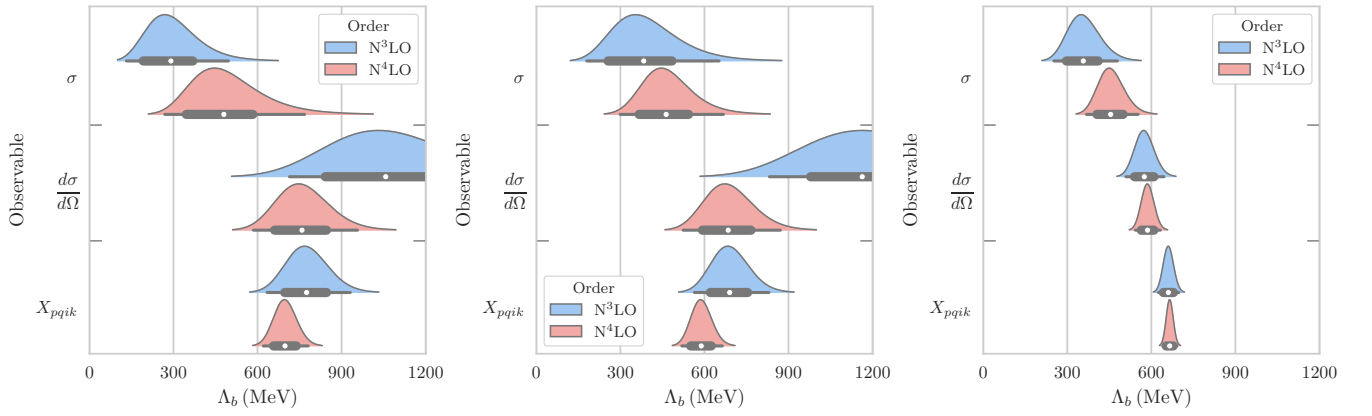


FIG. 20.  $\Lambda_b$  posterior plots generated using the  $R = 0.8$  fm EKM potential. Left, center, and right plots use  $E_{\text{lab}} = 96, 143, 200, 300$  MeV and  $\theta = 60^\circ, 120^\circ$ ;  $E_{\text{lab}} = 50, 96, 143, 200$  MeV and  $\theta = 60^\circ, 120^\circ$ ; and  $E_{\text{lab}} = 20, 40, \dots, 340$  MeV and  $\theta = 40^\circ, 60^\circ, \dots, 140^\circ$ , respectively.

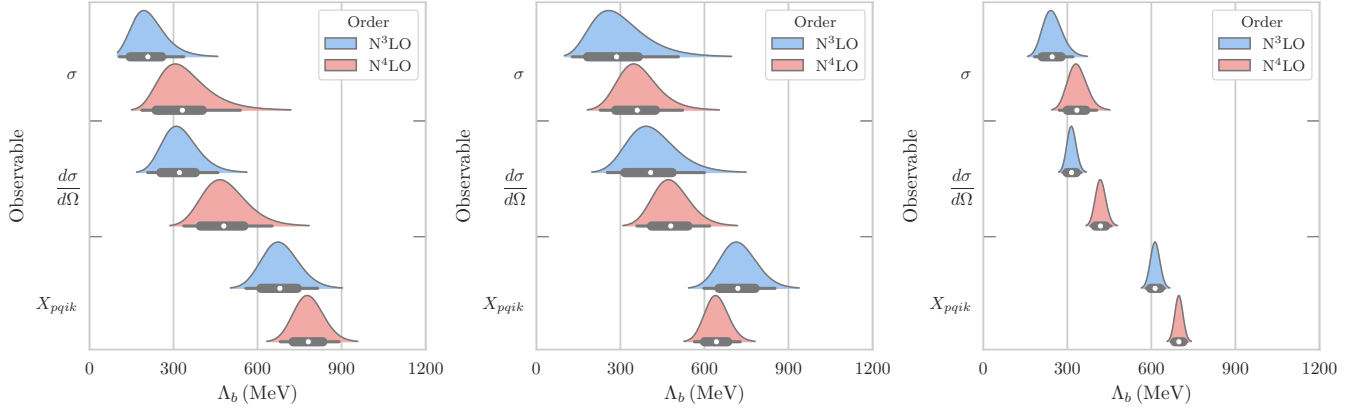


FIG. 21. Same as Fig. 20, but with the  $R = 1.0$  fm EKM potential.

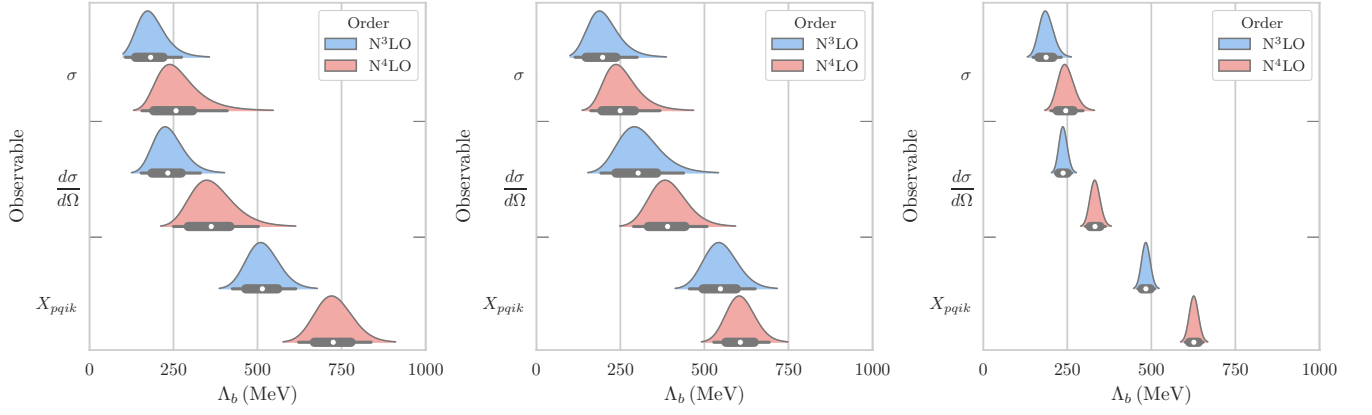


FIG. 22. Same as Fig. 20, but with the  $R = 1.1$  fm EKM potential.

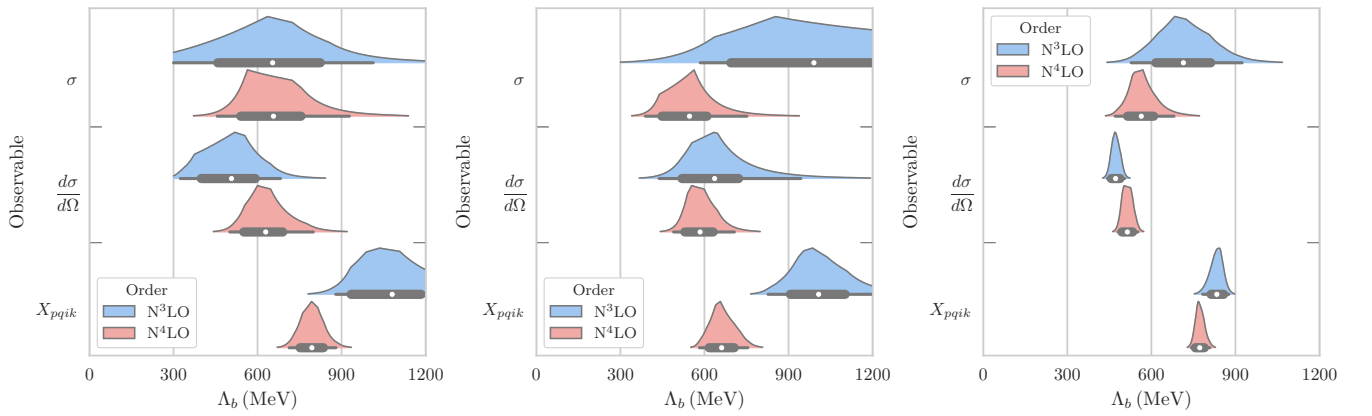


FIG. 23. Same as Fig. 20, but with the  $R = 0.9$  fm EKM potential and using set  $A_\epsilon$ .